

Control-oriented modelling for neoclassical tearing mode stabilization via minimum-seeking techniques

W. Wehner and E. Schuster

Department of Mechanical Engineering and Mechanics, Lehigh University, Bethlehem, PA 18015, USA

E-mail: wehner@lehigh.edu

Received 6 December 2011, accepted for publication 12 April 2012

Published 5 July 2012

Online at stacks.iop.org/NF/52/074003

Abstract

Suppression of magnetic islands driven by the neoclassical tearing mode (NTM) is necessary for efficient and sustained operation of tokamak fusion reactors. Compensating for the lack of bootstrap current, due to the pressure profile flattening in the magnetic island, by a localized electron cyclotron current drive (ECCD) has been proved experimentally as an effective method to stabilize NTMs. The effectiveness of this method is limited in practice by the uncertainties in the width of the island, the relative position between the island and the beam, and the ECCD power threshold for NTM stabilization. Heuristic search and suppress algorithms have been proposed and shown effective in improving the alignment of the ECCD beam with the island, using only an estimate of the island width. Making use of this estimate, real-time, non-model-based, extremum-seeking optimization algorithms have also been proposed not only for beam steering but also for power modulation in order to minimize the island-beam misalignment and the time required for NTM stabilization. A control-oriented dynamic model for the effect of ECCD on the magnetic island is proposed in this work to enable both control design and performance analysis of these minimum-seeking type of controllers. The model expands previous work by including the impact of beam modulation parameters such as the island-beam phase mismatch and the beam duty-cycle on the island width dynamics.

(Some figures may appear in colour only in the online journal)

1. Introduction

The onset of neoclassical tearing modes (NTMs) has been shown to limit the achievable plasma performance in tokamaks by enhancing heat transport, reducing energy confinement time and reducing the achievable β (plasma kinetic pressure/magnetic pressure) [1]. If the magnetic islands driven by NTMs were allowed to grow to their maximum saturated widths in ITER, recent simulations [2] indicate that they would cover about a third of the plasma and would reduce the potential fusion power production by about a factor of four. Therefore, stabilization of NTMs, which are expected to occur in reactor-grade tokamaks such as ITER, is one of the most critical issues in tokamak reactors since these modes seriously limit the high-pressure operation in long-pulse discharges.

The magnetic island is characterized by a locally flattened pressure profile, in which the pressure gradient is nearly absent. The consequent lack of bootstrap current drives the NTM instability and makes the island grow. Stabilization of the NTM can be achieved by localized deposition of an additional current that compensates for the locally declining bootstrap

current when an island grows [3, 4]. Electron cyclotron current drive (ECCD) has been proved experimentally in several tokamaks (ASDEX-U [5–7], DIII-D [8, 9], JT-60U [10]) as an effective method to stabilize NTMs. It has also been shown experimentally that broad-deposition modulated ECCD in phase with the island O -point and with a 50% (half on half off) duty-cycle is more efficient for mode stabilization than unmodulated (continuous) ECCD [11]. The ECCD effect on the island width dynamics has previously been studied numerically for the cases of continuous current drive and modulated current drive in phase with the island O -point using both static [12] and dynamic [13–15] models with different levels of sophistication. In this work these previous modelling results are expanded by including the effect of the island-beam phase mismatch. A control-oriented model based on the modified Rutherford equation [8], widely used to compute the time evolution of an island width, is proposed as both a control design and a simulation testing tool. The effects of ECCD beam position and power modulation on the NTM stabilization efficiency are incorporated into the model. All necessary parameters to fully describe the attributes of ECCD power

modulation are included in the model, i.e. the modulation duty-cycle (fractional on-time), phase mismatch between the ECCD ‘on-period’ and island O -point, and the difference between modulation frequency and island rotation frequency. The $q = m/n = 3/2$ NTM is considered in this paper, since, it is most often the first mode to significantly reduce confinement [16].

However, before current drive suppression can be used effectively in a reactor-grade plasma, several control challenges must be overcome. In particular, it may not be possible to accurately estimate the absolute position of the island or the relative position between the island and EC beam although some significant progress has been achieved recently. Often only a noisy estimate of the island width may be available in real time. Exploiting the availability of this real-time measurement, minimum-seeking control methods, such as search and suppress and extremum seeking, have been proposed to minimize the island width (and eventually suppress the island) by aligning the ECCD with the island and optimizing its modulation properties. The search and suppress method has been experimentally proved effective for real-time and sustained stabilization of both the 3/2 and 2/1 NTM (not simultaneously) in DIII-D [8, 17]. When the estimated island width exceeds a specified threshold, the search and suppress control algorithm enters into sweeping mode. During this mode, the plasma control system steers the ECCD launching mirror angle, produces small rigid radial position shifts of the entire plasma (and thus the island) or makes small changes in the toroidal field (and thus the ECCD location) to find and lock onto the optimum deposition location for complete island suppression by ECCD. The plasma control system thus executes a ‘blind search’ by changing the relative position between the island and the ECCD deposition location. A typical dwell time of 100 ms allows for checking if the mode amplitude decreases or not. If the mode does decrease, but at a rate slower than a specified threshold rate, a further step and dwell is made. Upon encountering a specified limit in the search parameter without satisfactory mode suppression, the search reverses direction. Once the mode is suppressed, the search and suppress control algorithm enters into freezing mode, where the plasma control system freezes the search parameter until such time as the mode reappears. The extremum-seeking method has recently been proposed for both beam steering and power modulation in order to minimize the island-beam misalignment and the time (control energy) required for NTM stabilization [18]. As a real-time, non-model-based, adaptive controller, the extremum-seeking algorithm provides a systematic way to optimize multiple parameters related to beam steering (misalignment), modulation (frequency, phase, duty-cycle) and quality (deposition width, power) simultaneously. Through well-engineered probing signals, the plasma control system perturbs these beam parameters to estimate in real time the gradient of the mapping defined between the ECCD parameters and the island width. By modifying the parameters in the direction opposite to the gradient the island is eventually suppressed.

Through a simulation study we illustrate in this work how the proposed control-oriented NTM response model can play an important role in testing the performance of

minimum-seeking ECCD control algorithms and in enhancing their effectiveness through proper tuning before experimental implementation. Both the search and suppress and extremum-seeking algorithms are implemented, analysed and compared in simulations. In addition, we also illustrate in this work how the proposed control-oriented model can be used to reduce the time (control energy) required for NTM stabilization even in the presence of model uncertainties. A nonlinear inversion of the control-oriented response model is complemented by an extremum-seeking loop, which is capable of overcoming the model uncertainties due to its non-model-based nature by fine-tuning the ECCD steering, modulation and quality parameters.

The paper is organized as follows. Section 2 describes the model proposed to compute the effect of ECCD on the island growth rate, which is analysed through an in-depth numerical study. Section 3 states the NTM control problem and describes both the search and suppress and extremum-seeking algorithms. Closed-loop simulation results based on minimum-seeking NTM stabilization methods are presented in section 4. Conclusions are summarized in section 5.

2. Island-beam interaction model

The growth dynamics of NTM islands in response to applied ECCD can be described by a form of the modified Rutherford equation [8, 9],

$$\frac{\tau_R}{r} \frac{dw}{dt} = \Delta' r + \epsilon^{1/2} \left[\frac{L_q}{L_p} \right] \beta_p \frac{r}{w} \left[\frac{w^2}{w^2 + w_d^2} - \frac{w_{pol}^2}{w^2} - K_1 \left(\frac{w}{w_{cd}}, \frac{\Delta R}{w_{cd}}, \tau, \xi \right) \frac{j_{cd0}}{j_{bs}} \right], \quad (2.1)$$

where w is the full island width, i.e. the radial scale length over which the pressure profile is assumed to be flattened, τ_R is the current diffusion time and r is the minor radius at which the NTM is resonant (the particular rational surface $q = m/n$). All the terms in equation (2.1) are dimensionless and the effects of magnetic field curvature (the Glaser–Green–Johnson effect) have been neglected.

On the right-hand side of equation (2.1) the classical tearing stability index Δ' is a property of the global plasma equilibrium; it represents the free energy available in the plasma current density to drive the tearing mode. If $\Delta' > 0$, there is free energy available for reconnection [19]. The equation

$$\frac{\tau_R}{r^2} \frac{dw}{dt} = \Delta' \quad (2.2)$$

defines the growth behaviour of the classical tearing mode which is linearly unstable ($\Delta' > 0$) when ideal MHD behaviour breaks down for a resistive plasma. However, Δ' becomes negative, the island becomes linearly stable, when the island width exceeds the resistive layer width which is far too small in present day tokamaks to be measured. In this work, we assume $\Delta' < 0$, so the island will be driven unstable by plasma pressure effects, i.e. it is a NTM we are considering. Additionally, in the limit of small islands ($w \ll r$), Δ' is not influenced by the presence of the island itself [20].

An initial seed island flattens the pressure gradient causing a helically perturbed bootstrap current which reinforces the island. This effect is described by the second term on the right-hand side of equation (2.1). Here, $\beta_p = 2\mu_0 p / B_p^2$ (poloidal

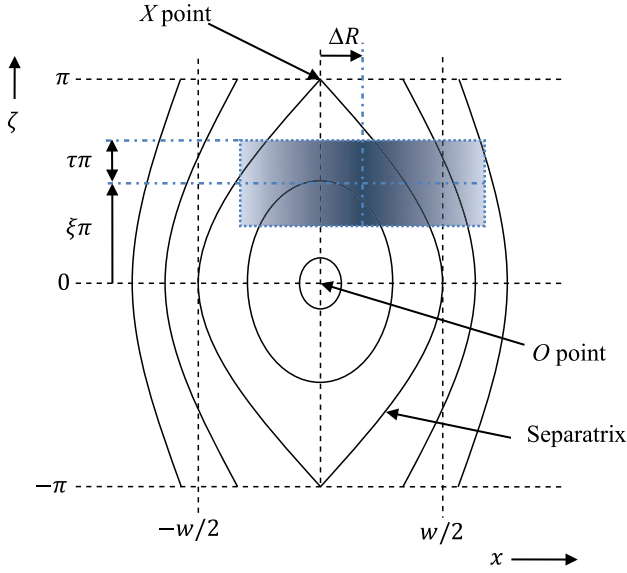


Figure 1. Contours of non-dimensional flux surface label ψ plotted in (x, ζ) space, where x is the radial distance from the rational surface and ζ is the helical angle.

β) is the ratio of plasma pressure p to the poloidal magnetic field pressure, where B_p is the poloidal magnetic field. The parameters $L_p \equiv -p/(dp/dr) > 0$, $L_q \equiv q/(dq/dr) > 0$ and $\epsilon = r/R_0$ are the pressure gradient length the magnetic shear length and the inverse aspect ratio, respectively. The characteristic transport effect island width w_d is associated with the parallel and perpendicular heat transport in the island. It relates to the fact that islands do not occur simultaneously on multiple rational q surfaces. It can also be described as the characteristic island width below which the pressure profile in the magnetic island is no longer fully flattened [8, 20]. The third term on the right-hand side of equation (2.1) represents the stabilizing effect of the ion polarization current, where w_{pol} is the characteristic island width associated with the helical polarization current arising from inertial effects [8]. The last term in equation (2.1) represents the stabilizing effect of the ECCD. The ratio j_{cd0}/j_{bs} is the peak EC current density normalized to the local equilibrium bootstrap current density. The function K_1 determines the effectiveness of the ECCD in stabilizing the NTM; it measures the overall efficiency of the ECCD with respect to the misalignment between beam and island and the ECCD power modulation.

Figure 1 shows contours of the non-dimensional helical flux function ψ plotted in (x, ζ) space, where x is the radial distance from the rational surface and $\zeta = m\theta - n\phi$ is the helical angle of the mode, with θ, ϕ, m, n denoting the poloidal and toroidal angles and mode numbers, respectively. An island of radial width w occurring on a rational surface with m poloidal windings is apparent. The island O -point, defined as the centre of the island at the helical angle corresponding to the maximum width of the island, is located at coordinates $(x = 0, \zeta = 0)$ and the island X -point is at $(x = 0, \zeta = \pm\pi)$. The flux function $\psi = 0$ represents the separatrix and $\psi = -1$ is at the island O -point. The shaded blue box represents the portion of the island over which ECCD power is deposited; throughout this paper it is referred to as the ‘on-period’. The box is darker in the middle to represent the Gaussian

distribution of radio frequency waves emitted by the gyrotrons, the source of the ECCD. The offset ΔR is the misalignment between the centre of the beam and the midpoint of island width ($x = 0$). The parameters τ and ξ correspond to the extension of the ECCD power deposition along the helical angle and the phase mismatch between the centre of the power deposition and the island O -point, respectively. The width w_{cd} is the full \exp^{-1} current density width of the driven current; it is related to the full width at half maximum (FWHM) δ_{ec} by $\delta_{ec}/w_{cd} = \sqrt{\ln(2)}$.

Following the work in [13, 21], we propose K_1 to be defined as

$$K_1 \left(\frac{w}{w_{cd}}, \frac{\Delta R}{w_{cd}}, \tau, \xi \right) = \frac{1}{C} \int_{-1}^{\infty} J \left(\psi, \frac{w}{w_{cd}}, \frac{\Delta R}{w_{cd}}, \tau, \xi \right) W(\psi) d\psi. \quad (2.3)$$

The non-dimensional helical flux function ψ , shown in figure 1, can be described as [13]

$$\psi = \frac{x^2}{(w/2)^2} - \left(\frac{1 + \cos(\zeta)}{2} \right), \quad (2.4)$$

where w is the full island width. The flux surface average quantities of (2.3) are

$$J \left(\psi, \frac{w}{w_{cd}}, \frac{\Delta R}{w_{cd}}, \tau, \xi \right) = \frac{1}{V(\psi)} \oint \frac{\tilde{j}_{cd} \left(\zeta, \psi, \frac{w}{w_{cd}}, \frac{\Delta R}{w_{cd}} \right) M(\zeta, \tau, \xi)}{\sqrt{\psi + \cos^2(\zeta/2)}} d\zeta, \quad (2.5)$$

$$W(\psi) = \oint \frac{\cos(\zeta)}{\sqrt{\psi + \cos^2(\zeta/2)}} d\zeta, \quad (2.6)$$

$$V(\psi) = \oint \frac{1}{\sqrt{\psi + \cos^2(\zeta/2)}} d\zeta, \quad (2.7)$$

where $M(\zeta, \tau, \xi)$ is the modulation function, $\tilde{j}_{cd}(\zeta, \psi, w/w_{cd}, \Delta R/w_{cd})$ is the normalized driven current profile, i.e. $j_{cd} = j_{cd0} \tilde{j}_{cd}(\zeta, \psi, w/w_{cd}, \Delta R/w_{cd})$ and j_{cd0} is the peak value. The contour integral \oint denotes the region $-\pi < \zeta < \pi$ for $\psi > 0$ and the interval where $\psi + \cos^2(\zeta/2) \geq 0$ for $-1 < \psi < 0$. The constant C is

$$C = \int_{-1}^0 W d\psi = 2.67. \quad (2.8)$$

We assume a Gaussian driven current density distribution in terms of x of the form

$$\tilde{j}_{cd} = \exp \left[-\frac{4(x - x_{dep})^2}{w_{cd}^2} \right], \quad (2.9)$$

where x_{dep} is the deposition location and, again, w_{cd} is the full \exp^{-1} driven current density width. Since, from equation (2.4), $x = \pm(w/2)\sqrt{\psi + \cos^2(\zeta/2)}$, the driven current density profile can be re-expressed as a function of (ψ, ζ) , i.e.

$$\tilde{j}_{cd} \left(\zeta, \psi, \frac{w}{w_{cd}}, \frac{\Delta R}{w_{cd}} \right) = \exp \left\{ -\left(\frac{\pm w}{w_{cd}} \sqrt{\psi + \cos^2(\zeta/2)} + 2 \frac{\Delta R}{w_{cd}} \right)^2 \right\}. \quad (2.10)$$

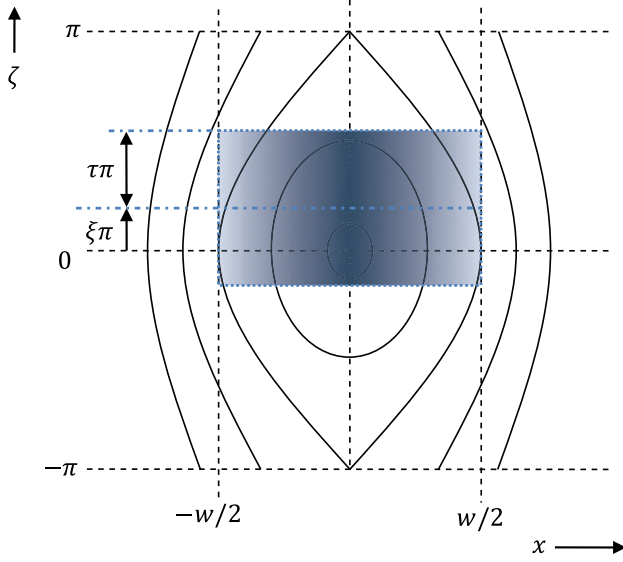


Figure 2. Case (i.): the ‘on-period’ modulation is driven entirely on a single island.

The modulation function M is defined as 1 over the helical angle during which the ECCD is turned on, i.e. the ‘on-period’, and 0 otherwise. In this work, M is expressed in terms of the phase mismatch between the ‘on-period’ and the O -point, ξ , and the EC power modulation factor, τ . As can be seen in figure 1, ξ is the phase mismatch and τ , which represents the percentage of the island covered by the ECCD, is related to the modulation duty-cycle. The parameters τ and ξ are defined on the ranges $0 \leq \tau \leq 1$, 1 corresponding to a continuous drive and 0 to an impulse, and $0 \leq \xi \leq 1$, 0 corresponding to the island O -point and 1 to the X -point.

To parametrize the modulation function in terms of τ and ξ , there are two cases to be considered: (i.) $\xi\pi + \tau\pi \leq \pi$, in which case the ‘on-period’ is located entirely on one island, as depicted in figure 2, and (ii.) $\xi\pi + \tau\pi > \pi$, in which case the ‘on-period’ overlaps from one island into the next, as depicted in figure 3. For case (i.) we define

$$M(\zeta, \tau, \xi) = \begin{cases} 1 & \xi\pi - \tau\pi \leq \zeta \leq \xi\pi + \tau\pi, \\ 0 & \xi\pi + \tau\pi < \zeta \leq \pi, \\ 0 & -\pi \leq \zeta < \xi\pi - \tau\pi, \end{cases} \quad (2.11)$$

while for case (ii.) we define

$$M(\zeta, \tau, \xi) = \begin{cases} 1 & \xi\pi - \tau\pi \leq \zeta \leq \pi, \\ 1 & -\pi \leq \zeta \leq (\xi\pi + \tau\pi) - 2\pi, \\ 0 & (\xi\pi + \tau\pi) - 2\pi < \zeta < \xi\pi - \tau\pi. \end{cases} \quad (2.12)$$

Now equation (2.3) is fully defined. However, there is no analytical solution for it and it is time-consuming to solve it numerically for a continuous range of its parameters. It is possible, nevertheless, to evaluate K_1 at certain intervals over a range of physically plausible values for $\Delta R/w_{cd}$, w/w_{cd} , τ , and ξ and to use linear interpolation of these evaluations for fast control-oriented simulations. Equation (2.1) is plotted in figure 4 for parameters typical of DIII-D discharges associated with the $m/n = 3/2$ NTM [8, 9]. From figure 4 we can appreciate that the NTM is linearly stable and nonlinearly

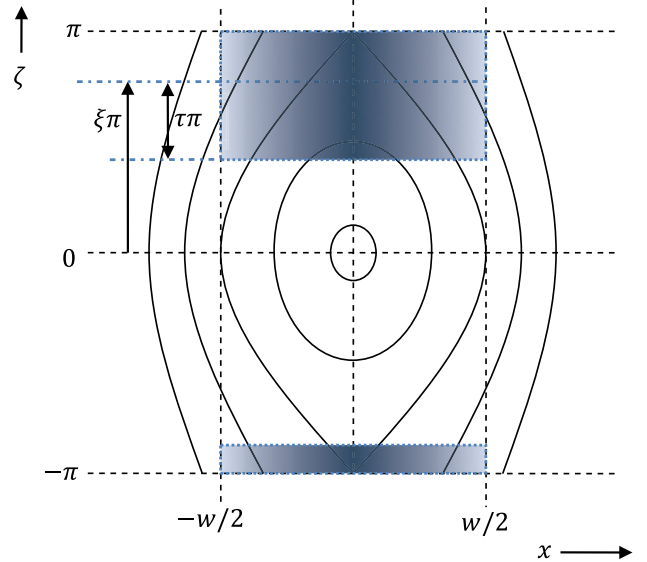


Figure 3. Case (ii.): the ‘on-period’ modulation is driven on two islands, overlapping from one island into the next.

unstable for no applied ECCD. To destabilize the NTM some mechanism is required to initiate a seed island and grow it beyond the critical island width (where the curve crosses zero from below) at which point the island continues to grow until reaching the saturated width w_{sat} . We can see that the island has a saturation size of $w_{sat} = 7.5$ cm when there is no applied ECCD.

If β_p is reduced, the entire growth rate curve will be lowered, and for sufficiently low β_p , the curve will be lowered completely below zero ensuring stability of the NTM [19]. Therefore the NTM can be stabilized by simply ramping down β_p . Unfortunately, this is an undesirable action in commercial-grade tokamaks. Instead, we can see from figure 4, that increasing the applied ECCD power can stabilize the NTM by essentially lowering the overall growth curve. For stabilization by ECCD, the beam must be sufficiently well aligned with the centre of the island. For instance, from figure 4 we can note that for $j_{cd0}/j_{bs} = 1$ the applied ECCD will fully stabilize the island as long as the misalignment is smaller than $\Delta R = 1.3$ cm. In the case of $\Delta R = 1.5$ cm, the applied ECCD can only shrink the island to 4.7 cm for this value of j_{cd0}/j_{bs} . With increasing displacement from the island centre more current is injected outside of the island, resulting in a destabilizing effect on the island.

The ECCD effectiveness K_1 is plotted as a function of w/w_{cd} in figure 5 (left) for unmodulated current drive ($\tau = 1$) and various ratios of misalignment to current drive width $\Delta R/w_{cd}$. The curves show a strong sensitivity to the $\Delta R/w_{cd}$ ratio. For instance, as the $\Delta R/w_{cd}$ ratio increases for $w/w_{cd} = 1$, the ECCD becomes destabilizing ($K_1 < 0$), reaches a point of maximum destabilization (minimum K_1) and eventually becomes neutral ($K_1 = 0$). This is clearly illustrated in figure 5 (right), where the ECCD effectiveness K_1 is replotted as a function of $\Delta R/w_{cd}$ for different values of w/w_{cd} . Thus, there will be a local minimum in the effectiveness K_1 as a function of $\Delta R/w_{cd}$, which can create difficulties for minimum-seeking control algorithms if not properly tuned. For example, assuming a fixed current drive width w_{cd} , if

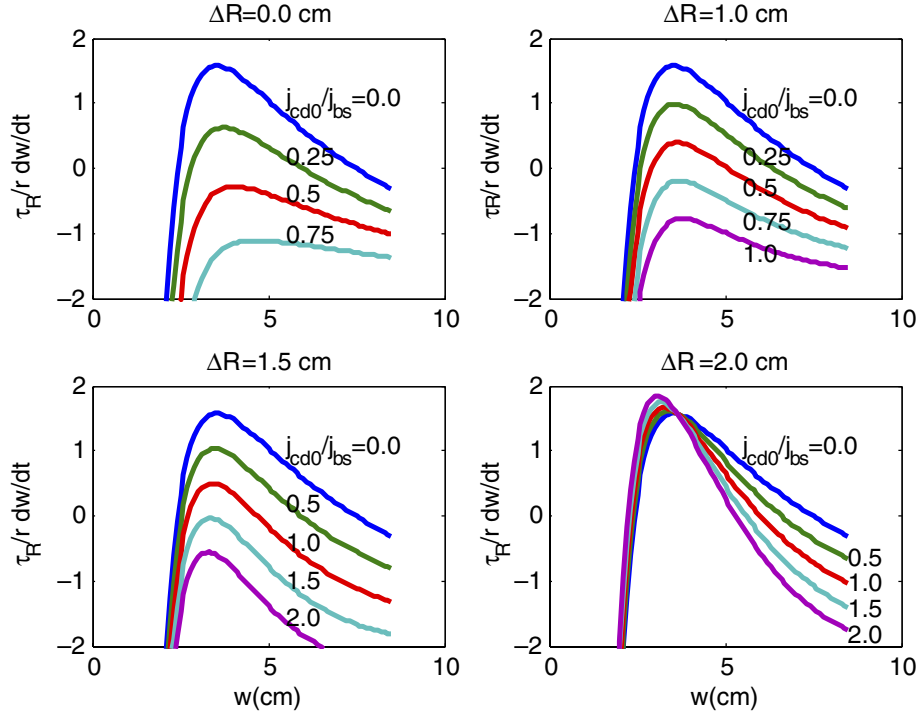


Figure 4. Normalized growth rate $(\tau_R/r)(dw/dt)$ as a function of full island width w and various values of driven current density j_{cd0} and misalignment ΔR . No ECCD modulation. The parameters of equation (2.1) are typical of DIII-D discharges associated with the $m/n = 3/2$ island: $\Delta r = -3$, $w_d = 1.01$ cm, $w_{pol} = 1.8$ cm, $w_{cd} = 3.46$ cm ($\delta_{ec} = 2.88$ cm), $r = 36$ cm, $\epsilon^{1/2} = 0.5$, $\beta_p = 0.9$, $L_q/L_p = 1.5$.

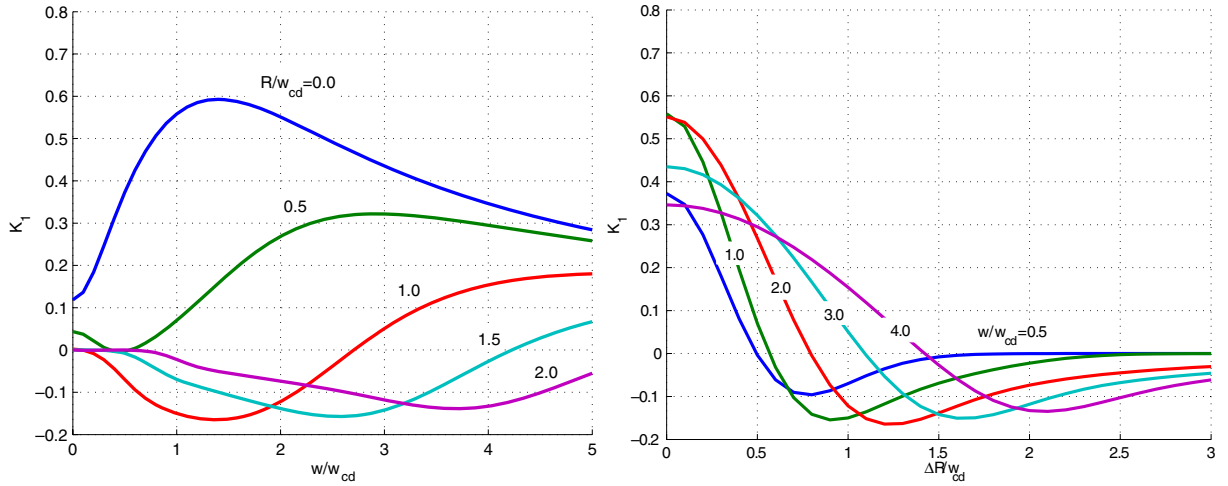


Figure 5. ECCD effectiveness K_1 for unmodulated current drive ($\tau = 1$) plotted as a function of w/w_{cd} for different values of $\Delta R/w_{cd}$ (left) and as a function of $\Delta R/w_{cd}$ for different values of w/w_{cd} (right). The left figure is similar to figure 2 in [9] with δ_{ec} replaced by w_{cd} .

the misalignment is beyond (to the right of) the point of minimum effectiveness, then moving the ECCD towards the island will actually cause the island to grow. After detecting the island growth the algorithm (extremum seeking or search and suppress) may move the ECCD away from the island. However, as the island width grows and w/w_{cd} increases, the local minimum shifts to the right. If the controller is tuned to make the alignment correction slower than the growth of the island, the misalignment will eventually find itself below (to the left of) the point of minimum effectiveness, allowing the control algorithm to drive the ECCD towards the centre of the island.

Figure 6 plots K_1 as a function of τ for various ratios of the current drive width w_{cd} to island width w . Note that for relatively wide ECCD current deposition ($w_{cd}/w > 2$), there is a well-defined maximum in the effectiveness at around $\tau \approx 0.5$. For a current drive deposition with the same width of the island ($w_{cd}/w = 1$), the maximum effectiveness is achieved at around $\tau \approx 0.6$. For relatively narrow ECCD current deposition ($w_{cd}/w < 1$) the maximum effectiveness seems to be achieved for higher τ values. Note, however, that as w_{cd}/w decreases, the sensitivity of the maximum value of the effectiveness with respect to τ also decreases. Therefore, it seems reasonable to adopt $\tau = 0.5$ as the approximate

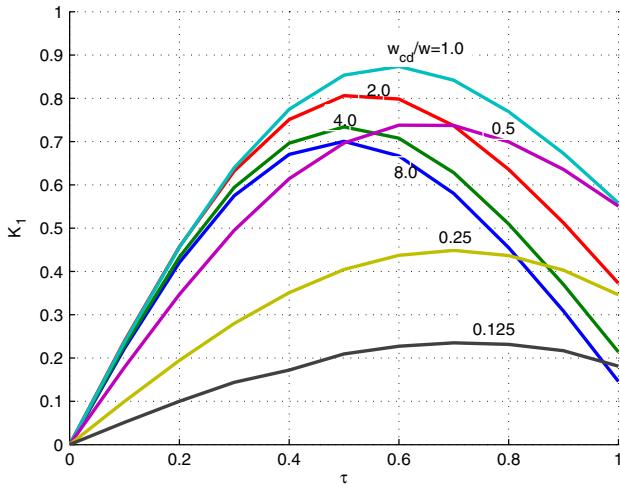


Figure 6. ECCD effectiveness K_1 plotted as a function of τ for various current drive width to island width ratios w_{cd}/w and O -point modulation ($\xi = 0$). There is no misalignment between the island and the current drive ($\Delta R = 0$).

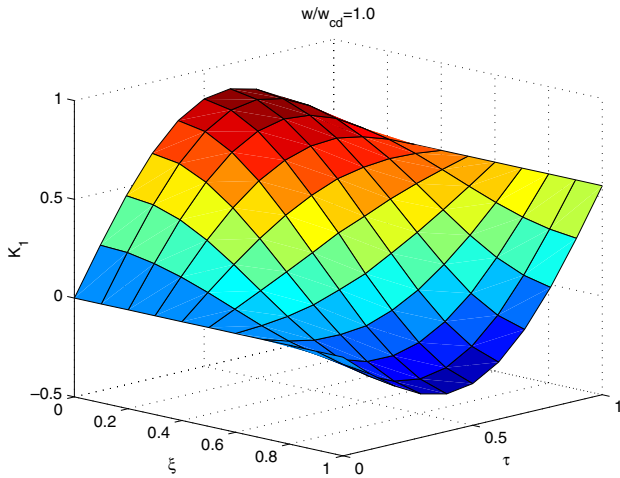


Figure 7. ECCD effectiveness K_1 as a function of τ and ξ for $w/w_{cd} = 1$ and $\Delta R = 0$.

optimizing value of the effectiveness for all w_{cd}/w ratios when we choose not to optimize τ in real time. As shown in figure 6, if perfect alignment and O -point modulation is guaranteed, the real-time optimization of τ will produce a relatively small increase in the effectiveness achieved for $\tau = 0.5$ regardless of the value of the w_{cd}/w ratio.

Figure 7 shows the combined effect of τ and ξ on K_1 for $w_{cd}/w = 1.0$ and zero misalignment ($\Delta R = 0$). The figures show the importance of setting the correct phase value when attempting to modulate the current drive. Tuning the modulation phase in real time will allow not only for the minimization of the suppression time but also for the avoidance of any potential destabilizing effect by the current drive. We note from figure 7 that modulated current drive applied in phase with the O -point ($\xi = 0$) is always stabilizing whereas current drive in phase with the island X -point ($\xi = 1$) may be destabilizing for some values of τ .

In figure 8, K_1 is plotted as a function of τ at various values of the phase mismatch ξ for the case characterized by $w/w_{cd} = 1$ (current drive width equal to island width) and

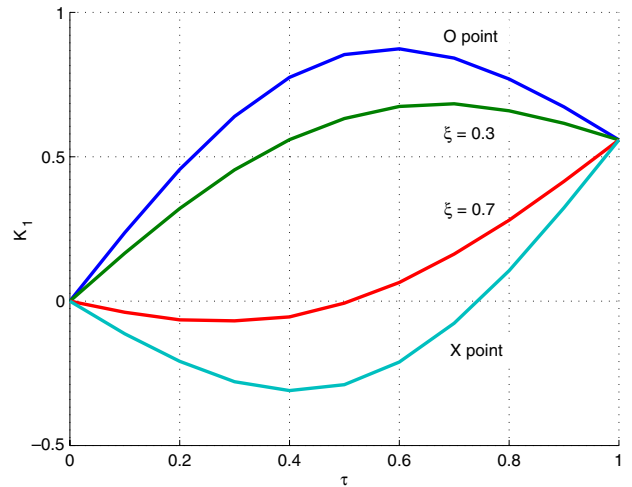


Figure 8. ECCD effectiveness K_1 plotted against τ for various values of ξ at $w/w_{cd} = 1$ and $\Delta R = 0$.

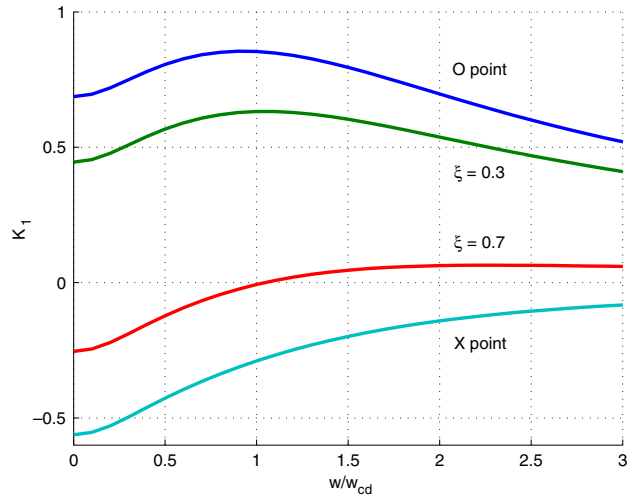


Figure 9. ECCD effectiveness K_1 plotted against w/w_{cd} for various values of ξ at $\tau = 0.5$ and $\Delta R = 0$.

$\Delta R = 0$ (zero misalignment). The effect of the current drive is maximized for $w/w_{cd} = 1$ as shown in figure 6. The O -point modulation is always stabilizing and has the greatest stabilizing effect, which is maximized at $\tau \approx 0.6$. The X -point modulation is destabilizing for $0 < \tau \lesssim 0.75$ and has the greatest destabilizing effect, which is maximized at $\tau \approx 0.4$. By examining figures 8 and 9 we can note that for $w/w_{cd} = 1$ the current drive effectiveness for a $\tau = 0.5$ modulation with phase mismatch of $\xi = 0.3$ is approximately that of a continuous drive ($\tau = 1$). Clearly, phase alignment is crucial when using modulated current drive.

In figure 9, K_1 is plotted as a function of the island width to current drive width ratio w/w_{cd} at various values of the phase mismatch ξ for the case of a $\tau = 0.5$ modulation and zero misalignment ($\Delta R = 0$). We can note that the effect of the current drive is maximized around $w/w_{cd} = 1$ when the modulation is approximately around the O -point (small ξ). For $w/w_{cd} > 1$, the effect of the current drive on the island diminishes with increasing w/w_{cd} ratio, i.e. for O -point modulation the current drive has less stabilizing effect and

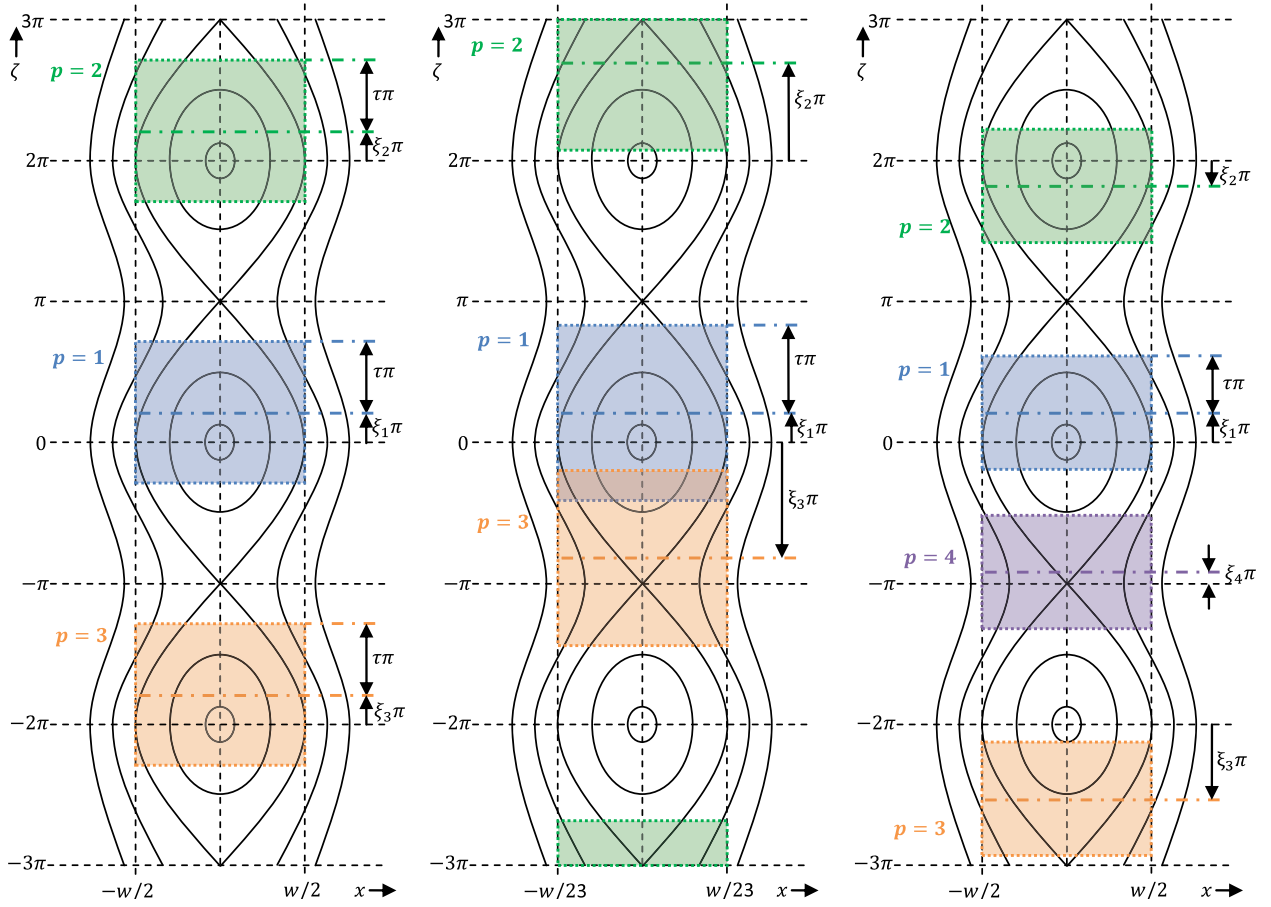


Figure 10. Several cases of 50/50 duty-cycle modulation ($d = 0.5$). We assume the islands are moving down the page. The boxes represent the portion of the island over which ECCD power is injected. The first ‘on-period’ is marked by $p = 1$, the second by $p = 2$, etc. The first case (left) shows ECCD power modulation in sync with the island rotation frequency ($f_r = 1$, $\tau = d$), where ξ remains constant ($\xi_1 = \xi_2 = \xi_3$). The second case (middle) shows a power modulation frequency slower than the island rotation frequency, $f_r = 0.8 < 1$. In this case τ is larger than d and the phase mismatch ξ changes with time. The third case (right) shows a power modulation frequency faster than the island rotation frequency, $f_r = 1.2 > 1$. In this case, τ is smaller than d and the phase mismatch ξ changes with time. In each case the length of the ‘on-period’ box in terms of ζ is equal to the length of spacing (‘off-period’) between boxes since we are considering 50/50 duty-cycle modulation.

for X-point modulation the current drive has less destabilizing effect for increasing w/w_{cd} ratio. Once again, phase alignment is shown to be crucial when using modulated current drive.

It is important to recognize that the parameters τ and ξ are dependent on the ECCD power modulation frequency. If the power modulation frequency is in sync with the island rotation frequency, τ and ξ remain constant. Otherwise, τ and ξ become functions of time and the ratio between the two frequencies, i.e. $\tau = \tau(f_r)$ and $\xi = \xi(t, f_r)$, where f_r denotes the ratio of ECCD power modulation frequency f to island rotation frequency Ω , i.e. $f_r = f/\Omega$. When the two frequencies are in sync ($f_r = 1$), τ is equivalent to the ECCD power modulation duty-cycle d . This fact is quite clear from figure 10 (left), where the boxes representing the ‘on-period’ cover a proportion of the island exactly equal to d . For the case of 50/50 duty-cycle modulation shown in the figure, the length of the boxes along ζ is equal to the length of spacing between the boxes since $\tau = d = 0.5$. For a greater fractional ‘on-period’ with $d > 0.5$, the length of the boxes expands and the spacing between boxes shrinks proportionately; the converse occurs for $d < 0.5$. If there is a discrepancy between

the two frequencies ($f_r \neq 1$), τ becomes linearly related to the frequency ratio by $\tau = d/f_r$. This is somewhat apparent from figure 10 (middle and right), where both cases consider 50/50 duty-cycle modulation, implying equal length of the boxes and the spacing between the boxes. When the modulation frequency is slower than the island rotation rate ($f_r < 1$) the boxes along ζ appear expanded in comparison with the $f_r = 1$ case. Conversely, the boxes along ζ appear shortened in the $f_r > 1$ case.

Since each ‘on-period’ occurs every $1/f$ seconds, the time t associated with the ‘on-period’ p can be denoted by $t_p = p/f$ and the phase ξ after p on-periods can be written as

$$\xi_p = \xi_1 + 2\Omega t_p = \xi_1 + 2p\Omega/f = \xi_1 + 2p/f_r, \quad (2.13)$$

where ξ_1 is the initial phase mismatch between the island and beam corresponding to the first ‘on-period’. Since ζ is periodic with period 2π , ξ is periodic with period of 2. Therefore, when $f_r = 1$, ξ remains constant and equal to its initial value ξ_1 , which is evident from figure 10 (left). When $f_r \neq 1$, ξ changes over time by shifts of $2/f_r$ for each consecutive ‘on-period’ p as can be noted from figure 10 (middle and right).

If the EC beam modulation frequency is not matched to the island rotation frequency, the current drive will repeatedly shift from O -point to X -point phase alignment resulting in a weaker effect of the ECCD power modulation on the island width. Precise tuning of the modulation frequency is therefore crucial for optimum current drive effectiveness. In this work, we simply assume that a method is available to determine the island rotation rate and that a dedicated controller is used to ensure that the beam modulation frequency matches this rate. Otherwise, the effect of the beam modulation (τ and ξ) on its effectiveness will be very weak on average. Electron cyclotron emission (ECE) has recently been proved effective in measuring the plasma temperature fluctuations around the island and using them to determine island rotation rate [22]. Once the island rotation rate is known, its synchronization with the beam modulation frequency becomes relatively straightforward. Thus, in this work we are only concerned with the control of the spatial mismatch ΔR , the phase mismatch ξ and the ECCD power modulation duty-cycle τ ($f_r = 1$).

3. Minimum-seeking control of NTMs

As discussed above, the NTMs can be stabilized by replacing the missing bootstrap current by ECCD. Alignment of the ECCD with the island must be achieved with great accuracy for the NTM suppression to be successful. However, real-time reconstruction of the plasma geometry can only locate the island with an accuracy of 1.5–2.0 cm [17]. Therefore, the position of the island is usually not available for NTM control. Neither is a precise estimation of the current deposition location. However, a relative measurement of alignment between island and current drive can be determined by modifying the ECCD deposition location and measuring the resulting change in island amplitude. Sweeping the ECCD along the plasma will cause the island to shrink as the deposition location nears the island centre and to grow back to its saturated size as the deposition location moves away.

3.1. Search and suppress control algorithm

The most common and successful sweeping approach to NTM stabilization is the search and suppress method [17]. The search and suppress algorithm, summarized in figure 11, steers the beam in a stepwise search to find the optimum ECCD deposition location. Once the control is enabled, the algorithm fixes the beam deposition location for a specified dwell time to assess the effect on the magnetic island. If the width of the island decreases by a pre-specified threshold, the algorithm continues to hold the beam deposition location fixed for an additional dwell time. Otherwise, the beam is steered in a step fashion and then held for a subsequent dwell period. If the beam position reaches a specified maximum, the step steering direction is reversed (a possible modification of this algorithm consists in reversing the step steering direction if the width of the island does not decrease by the pre-specified threshold for three consecutive step changes). The search-dwell-search procedure continues until the NTM is suppressed. Note that an accurate absolute estimate of the island width is not necessary since it is indeed the island reduction rate that is used as an indication of the quality of the beam-island alignment.

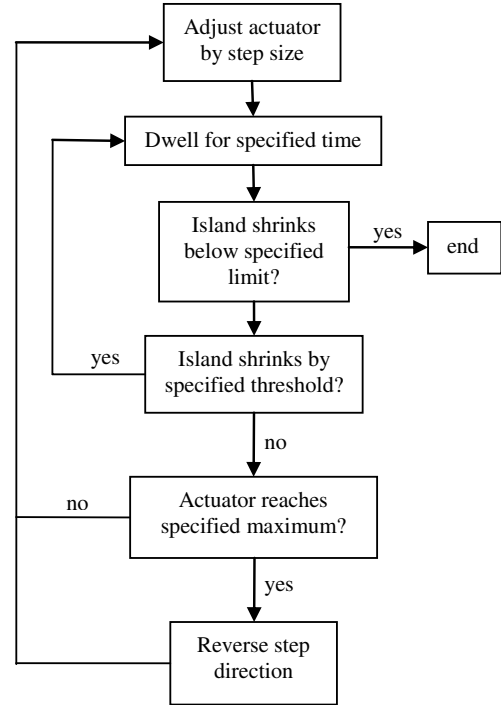


Figure 11. Search and suppress algorithm.

3.2. Extremum-seeking control algorithm

The extremum-seeking control method [23] is applicable to situations where there is a nonlinearity in the control problem, and the nonlinearity has a local minimum or maximum. Typical methods of adaptive control are useful only for regulation to a well-known set point. In many applications, however, the set point is unknown and should be selected to achieve either a minimum or a maximum of an uncertain parameter-to-output equilibrium map. If this map is uncertain, some adaptation is necessary to find the values of the parameters that minimize or maximize the output. This control problem is called ‘extremum control’ or ‘self-optimizing control.’ It is applicable to problems requiring the optimization of a multidimensional parameter space. Furthermore it is a non-model-based approach, i.e. it requires no explicit information of the system to determine the optimal parameter set points.

The modified Rutherford equation (2.1) can be rewritten as a general nonlinear model

$$\dot{w} = f(w, \theta), \quad (3.1)$$

$$y = h(w) = w, \quad (3.2)$$

where $w \in \mathfrak{R}$ is the state, $y \in \mathfrak{R}$ is the output, $\theta \in \mathfrak{R}^n$ is a vector parameter and $f : \mathfrak{R} \times \mathfrak{R}^n \rightarrow \mathfrak{R}$ and $h : \mathfrak{R} \rightarrow \mathfrak{R}$ are nonlinear smooth functions. In our case, $n = 3$ and $\theta = [\Delta R \quad \xi \quad \tau]^T$. Note that in this work both the peak intensity j_{cd0} and width w_{cd} of the ECCD beam are assumed constant, but they can be easily incorporated into the vector θ as to be optimized parameters.

Assumption 3.1. *There exists a smooth function $g : \mathfrak{R}^n \rightarrow \mathfrak{R}$ such that*

$$f(w, \theta) = 0 \iff w = g(\theta) \quad (3.3)$$

Moreover, for each $\theta \in \mathfrak{R}^n$, one of the equilibria $w = g(\theta)$ of system (3.1) is locally exponentially stable. The stable equilibrium is denoted as w_s .

As shown in figure 4, the modified Rutherford equation predicts two equilibria when the island is formed. The lower equilibrium width, w_m , is unstable, while the higher equilibrium width, w_s , is stable. The stable equilibrium width, w_s , corresponds to the saturated island width. The objective is to tune the parameter vector θ to drive w_s towards w_m , minimizing in this way the saturated island width and pushing the island into its stable regime where the width shrinks to zero.

Assumption 3.2. *There exists $\theta^* \in \mathfrak{R}^n$ such that*

$$(h \circ g)'(\theta^*) = 0, \quad (3.4)$$

$$(h \circ g)''(\theta^*) > 0. \quad (3.5)$$

Therefore, we assume that the output equilibrium map $y = h(g(\theta)) = g(\theta)$ has a minimum at $\theta = \theta^*$ in which $w_m = w_s$.

Our objective is to develop a feedback mechanism that drives the saturated island width w_s below its critical value w_m without requiring the knowledge of either θ^* or the functions f , g and h . Such mechanism is depicted in figure 12, where a continuous-time variant of extremum seeking [24] is adopted. The extremum-seeking controller uses a slow periodic perturbation $a \sin(\omega t)$ added to the signal $\hat{\theta}$, which represents the estimate of θ^* . If the perturbation is slow enough, then the plant (3.1)–(3.2) can be seen as a static map $J(\theta) \triangleq h \circ g(\theta) = g(\theta)$ representing the saturated island width as a function of the parameter vector θ . The minimum of J is denoted by J^* and its argument by θ^* . The objective is to minimize J . The perturbation signal $a \sin(\omega t)$ forces a periodic response in $J(\theta)$ which will be either in phase or out of phase with the perturbation signal. The high-pass filter $s/(s + \omega_h)$ (s denotes the Laplace transform variable) removes the dc component of $J(\theta)$, thus J_f will be approximately sinusoidal and v will be the product of two sinusoids that are either in phase ($\hat{\theta} < \theta^*$) or out of phase ($\hat{\theta} > \theta^*$). The low-pass filter $\omega_l/(s + \omega_l)$ then extracts the dc component of v , which will be positive if the two sinusoids are in phase and negative if they are out of phase. The sign of χ provides the direction to the integrator which tunes $\hat{\theta}$ to the optimal operating point θ^* . The closed-loop system of figure 12, for the case of $\phi = 0$, can be summarized as

$$\begin{aligned} \dot{J}_f &= -\omega_h J_f + J, \quad v = J_f b \sin(\omega t), \quad \dot{\chi} = -\omega_l \chi + \omega_l v, \\ \dot{\hat{\theta}} &= -\gamma \chi, \quad \theta = \hat{\theta} + a \sin(\omega t). \end{aligned} \quad (3.6)$$

The cutoff frequencies of the filters need to be lower than the frequency ω of the perturbation signal. Therefore, the overall feedback system has three time scales: (i) fast (plant), (ii) medium (periodic perturbation), (iii) slow (filters in extremum-seeking scheme). In addition, to guarantee local stability, the perturbation amplitudes a and b and the adaptation gain γ need to be small.

In our simulation studies we use (2.1) to predict the evolution of the island width for a given parameter vector θ . The saturated magnetic island width is considered as the cost functional (J in figure 12) and the extremum-seeking adaptive controller is used to optimally tune those parameters

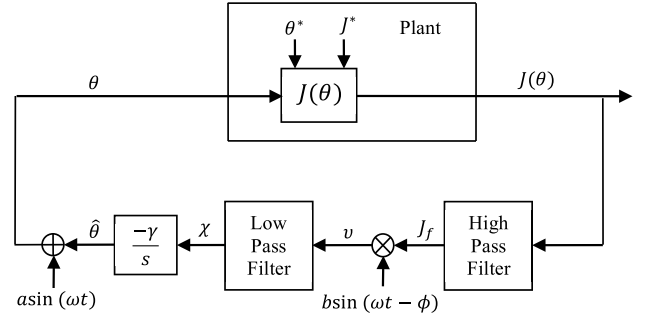


Figure 12. Extremum-seeking control scheme.

(θ in figure 12) affecting the stabilization of the NTM such as ΔR , τ , and ξ in order to suppress the island. Note that the dynamic model (2.1) is only necessary to carry out the simulation study presented in this paper, and no model of the plant is required when the extremum-seeking adaptive controller is implemented in a real tokamak.

The time to converge to the island centre may be further reduced using the modified Rutherford model (2.1) to estimate an approximate absolute value of the misalignment based on measurements of the island width and instantaneous growth rate, and using this estimate to correct the current drive deposition location. The implementation of extremum seeking with the accelerator [25] is shown in figure 13. The additional term μ is generated to decrease the difference between θ^* and $\hat{\theta}$, where an estimate of θ^* is determined by the optimal input identification block. The block is built around a nonlinear inversion of the modified Rutherford model (2.1), which uses noisy measurements of the island width and instantaneous growth rate to infer the beam-island misalignment ΔR and to estimate the optimal steering parameter θ^* that would be associated with perfect alignment ($\Delta R = 0$). Basically, coarse adjustments are made by the accelerator and finer adjustments are made by the extremum-seeking loop. By exploiting its non-model-based character and therefore natural robustness against model uncertainties, extremum seeking corrects any error in the estimate produced by the model inversion due to the uncertainty in the model. Since the difference $\hat{\mu} = \theta^* - \hat{\theta}$ carries the measurement noise, the adjustment in θ due to $\hat{\mu}$ may be somewhat violent. Therefore, a Butterworth filter is used to smooth down the violent movements in $\hat{\mu}$ for improved control.

4. Closed-loop simulation study

The ability of the control-oriented model proposed in section 2 to predict the island width evolution in response to the ECCD actuation is illustrated in a closed-loop simulation study. Both the search and suppress and the extremum-seeking algorithms discussed in section 3 are implemented and analysed. The simulation study is based on the model parameters given in figure 4 and the assumption that $j_{cd0}/j_{bs} = 1$. A 10% proportional noise is assumed to affect the island width measurement. A filtered version of the noisy measurement obtained by averaging the last seven samples is used for both algorithms. The sampling time is 1/40 of the dwell time for search and suppress and 0.001 s for extremum seeking.

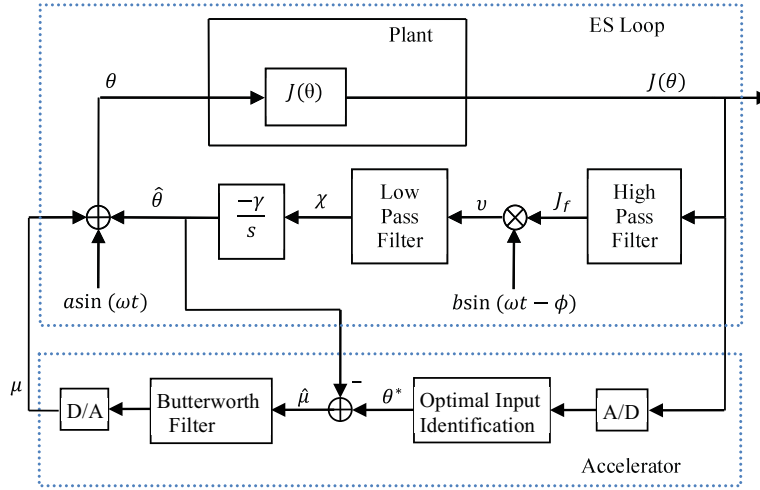


Figure 13. Extremum-seeking control scheme with accelerator.

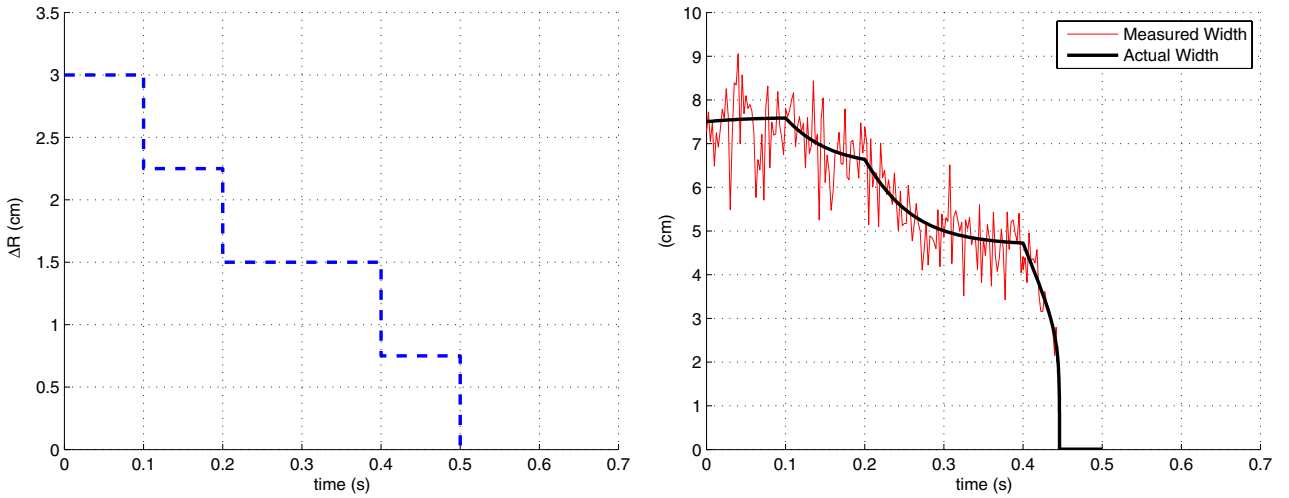


Figure 14. Search and suppress simulation with unmodulated current drive ($\Delta R_0 = 3.0$ cm): (left) misalignment ΔR ; (right) island width w : actual (black) and measured (red) width.

Figure 14 shows the performance of the search and suppress algorithm detailed in section 3.1 with unmodulated (continuous) current drive. The actuator step size is 0.75 cm, the dwell time is 100 ms, the initial saturated island width is 7.5 cm, and the initial misalignment is $\Delta R_0 = 3.0$ cm. The algorithm does not apply a hold until the third step when the rate of shrinking is rather substantial; it successfully stabilizes the island in just five dwell times. The suppression time could be reduced by increasing the actuator step size, but that would pose the risk of skipping over the island centre.

The search and suppress algorithm, whose performance is shown in figure 14 just for one simulation case, stabilizes the NTM with an average suppression time of $m = 0.48$ s and standard deviation of $\sigma = 0.06$ s when the initial misalignment is $\Delta R_0 = 3.0$ cm and there is no modulation of the current drive. With 50/50 duty-cycle *O*-point modulation the average suppression time would be reduced to $m = 0.36$ s with standard deviation $\sigma = 0.05$ s. However, it is important to emphasize at this stage that the search and suppress algorithm does not have the capability of controlling the modulation duty-cycle and phase (τ and ξ). A separate dedicated controller for modulation regulation would be necessary in this case.

The results above assume that the initial relative position between island and current drive is known, i.e. we know in what direction the beam must be moved to converge toward the island. If this information is not available, the initial step direction for the beam must be chosen randomly. In this case the suppression time increases to $m = 0.62$ s with $\sigma = 0.14$ s for no modulation and $m = 0.50$ s with $\sigma = 0.18$ s for 50/50 duty-cycle *O*-point modulation when the initial misalignment is $\Delta R_0 = 3.0$ cm. If the initial misalignment is chosen randomly in the range $0 < \Delta R < 3.0$ cm, then the average suppression time is $m = 0.46$ s with $\sigma = 0.35$ s for no modulation and $m = 0.39$ s with $\sigma = 0.35$ s for 50/50 duty-cycle *O*-point modulation. In all these simulation cases the standard search and suppress algorithm described in section 3.1 has been modified in order to reverse the steering direction if the island width increases by a specified rate after a single dwell time.

Figure 15 shows the performance of the extremum-seeking algorithm detailed in section 3.2, and illustrated in figure 12, for an unmodulated (continuous) current drive. We consider first the case where only one parameter is optimized; the misalignment $\theta = \Delta R$ (in practice the optimized parameter

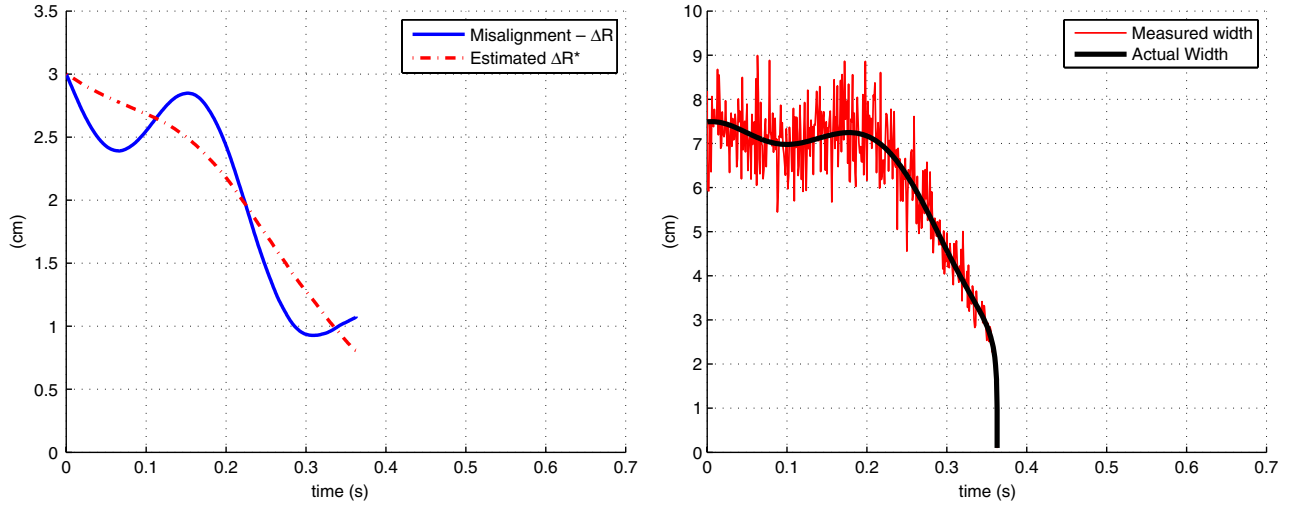


Figure 15. Extremum-seeking simulation with gain scheduling using unmodulated current drive ($\Delta R_0 = 3$ cm): (left) actual misalignment $\theta = \Delta R$ (solid), estimate $\hat{\theta}$ of optimal misalignment ΔR^* (dashed); (right) island width: actual (black) and measured (red) width.

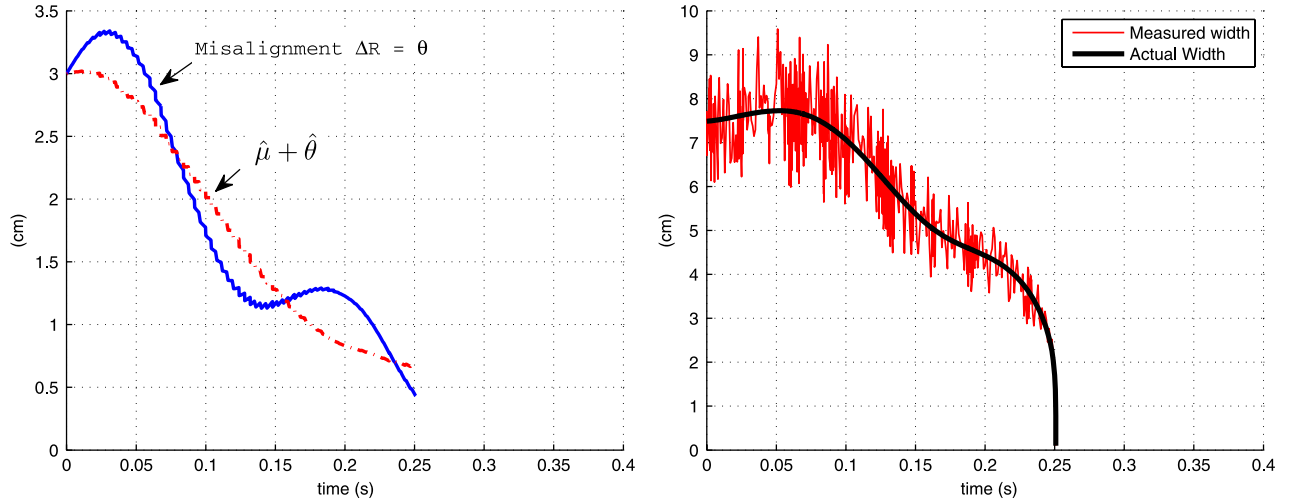


Figure 16. Extremum-seeking simulation with accelerator using unmodulated current drive ($\Delta R_0 = 3$ cm): (left) actual misalignment $\theta = \Delta R$ (solid), estimate $\hat{\theta}$ of optimal misalignment ΔR^* (dashed); (right) island width: actual (black) and measured (red) width.

is the beam deposition location, i.e. the beam steering). This case study allows for direct comparison with the search and suppress algorithm. The extremum-seeking parameters are selected for optimal suppression time. The modulation and demodulation amplitudes are $a = b = 0.4$ cm, the perturbation frequency is $\omega = 28$ rad s⁻¹, and the demodulation phase $\phi = 0.29$ rad to account for the phase shift due to the plant and the high-pass filter. Third order Butterworth filters are used in place of the typical first order linear filters to speed up the dynamics. The adaptation gain is chosen to be adjusted according to a linear interpolation from $\gamma = 150/b$ dB at $w = w_s = 7.5$ cm to $\gamma = 20/b$ dB at $w = w_m = 2.5$ cm, where w_m is the seed island width without current drive. The average suppression time when the initial misalignment $\Delta R_0 = 3.0$ cm is reduced to $m = 0.40$ s with standard deviation $\sigma = 0.07$ s for unmodulated current drive and to $m = 0.36$ s with standard deviation $\sigma = 0.08$ s for 50/50 duty-cycle O -point modulated current drive.

Figure 16 shows the performance of the extremum-seeking algorithm with modified Rutherford model-based

accelerator also discussed in section 3.2, and illustrated in figure 13, for an unmodulated (continuous) current drive. The perturbation frequency, probing signal magnitude, adaptation gain, and demodulation phase are $\omega = 40$ rad s⁻¹, $a = b = 0.4$ cm, $\gamma = 40/b$ dB, $\phi = 0.47$ rad, respectively. The accelerator samples at a rate of 0.005 s and the optimal input θ^* is updated at the same rate. The third order Butterworth cutoff frequency is $\omega_c = 15$ rad s⁻¹. The average suppression time when $\Delta R_0 = 3.0$ cm is reduced to $m = 0.25$ s with standard deviation $\sigma < 0.01$ s. With 50/50 duty-cycle O -point modulation the suppression time is reduced to $m = 0.21$ s with standard deviation $\sigma < 0.01$ s. When a random error of 10% is added to the parameters τ_R , Δ' , β_p , ω_d , ω_{pol} in (2.1), the suppression time increases to $m = 0.275$ s with standard deviation $\sigma < 0.025$ s for an unmodulated current drive, which is still significantly faster than conventional search and suppress and extremum-seeking algorithms. This illustrates how even an imperfect model can be exploited to improve the control efficiency. In general, embedding in the control design process the available information of the system dynamics given

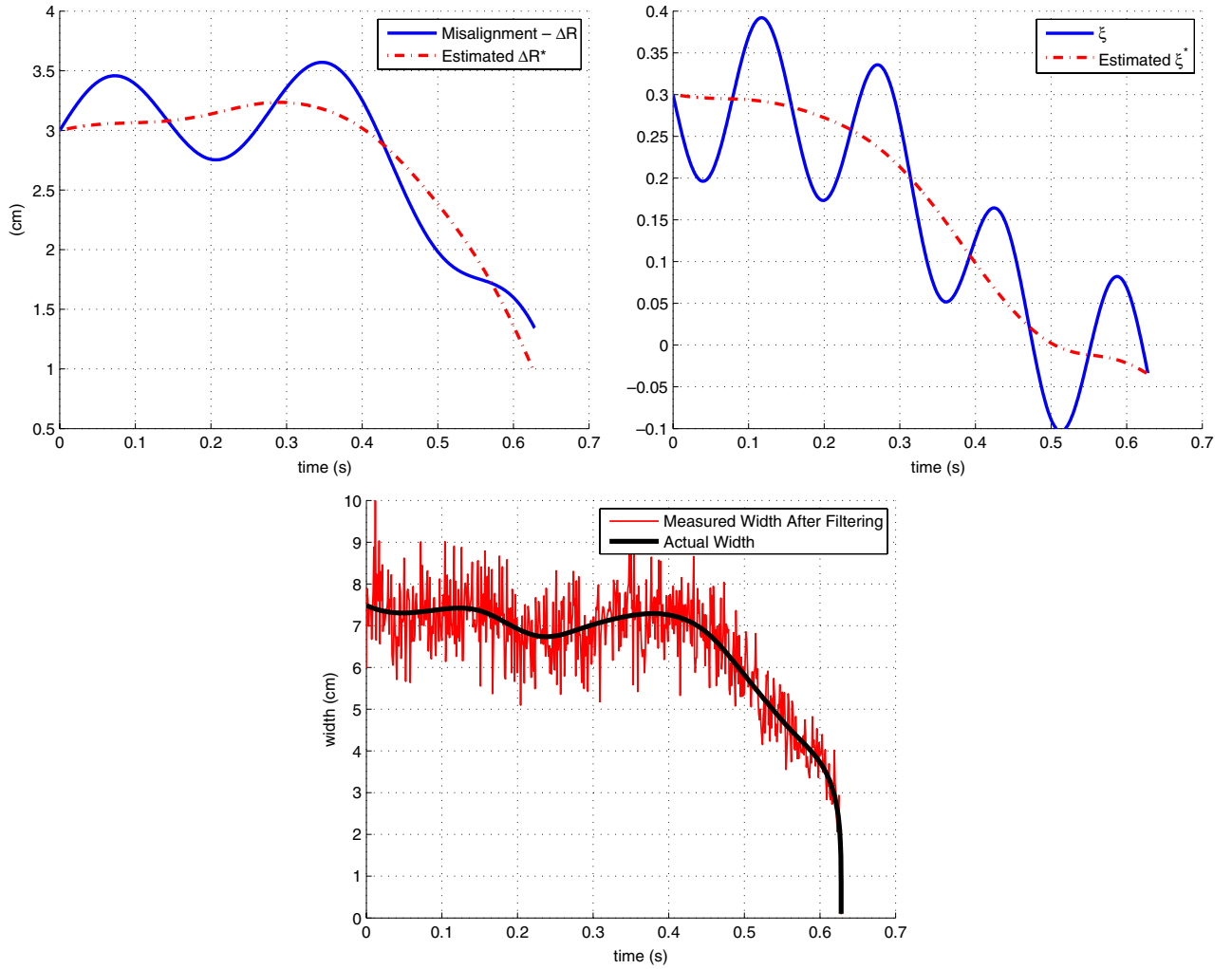


Figure 17. Two-parameter extremum-seeking (basic method) simulation with modulated current drive ($\Delta R_0 = 3$ cm, $\xi_0 = 0.3$): (left) actual misalignment $\theta_1 = \Delta R$ (solid), estimate $\hat{\theta}_1$ of optimal misalignment ΔR^* (dashed); (middle) actual modulation phase mismatch $\theta_2 = \xi$ (solid), estimate $\hat{\theta}_2$ of optimal phase mismatch ξ^* (dashed); (right) island width: actual (black) and measured (red) width.

by the model, regardless of how accurate or approximate it is, results in improved closed-loop performance.

Proper application of modulated current drive for stabilization of NTMs requires that we chose the correct modulation phase/duty-cycle for the optimal O -point modulation or else the efficiency improvement over continuous current drive will not be fully realized. The simulation cases illustrated in figure 15 (extremum seeking with gain scheduling) and figure 16 (extremum seeking with modified Rutherford model-based accelerator) assumed that optimal modulation was already achieved in order to focus only on misalignment correction for direct comparison with the search and suppress algorithm. Assuming no knowledge of the actual modulation phase/duty-cycle, we illustrate through the following simulation case how the extremum-seeking algorithm, unlike the search and suppress algorithm, can also be used to optimally control both the phase and the duty-cycle of the ECCD power modulation.

For instance, we consider now the case where two parameters are optimized by extremum seeking; the misalignment $\theta_1 = \Delta R$ and the phase mismatch $\theta_2 = \xi$ (the actual phase mismatch is $\xi\pi$ as depicted in figure 1).

The extremum-seeking parameters for the misalignment are identical to those used in figure 15 except the perturbation frequency is reduced to $\omega_1 = 22$ rad s $^{-1}$; the parameters for the phase mismatch are $a_2 = b_2 = 0.1$, $\gamma_2 = -2500/b$ dB, and $\omega_2 = 50$ rad s $^{-1}$. All the simulations assume a duty-cycle of 50/50 ($\tau = 0.5$), which represents the approximated optimum for all w/w_{cd} ratios (see figure 6). Figure 17 shows the performance of the basic extremum-seeking method (no gain scheduling or accelerator) for a modulated current drive. As can be noted from figure 17 (middle) the phase mismatch can be well adjusted to the optimal O -point location while simultaneously adjusting the misalignment. The average suppression time is $m = 0.62$ s with standard deviation $\sigma = 0.1$ s for $\Delta R_0 = 3$ cm and $\xi_0 = 0.3$. Had the phase not been adjusted from the initial value of $\xi_0 = 0.3$, the current drive would still have stabilized the NTM, but correcting the phase allows for a faster suppression time.

The results of the various simulations for the one-parameter (ΔR) optimization case are summarized in table 1 for continuous drive and 50/50 duty-cycle O -point modulated drive. The columns are from left to right the search and suppress algorithm, the extremum-seeking algorithm and the

Table 1. Comparison of various suppression methods for one-parameter (ΔR) optimization.

	SS	ES	ES(accel)
No mod	0.62 (0.14)	0.40 (0.07)	0.25 (<0.01)
O-point	0.50 (0.18)	0.36 (0.08)	0.21 (<0.01)

extremum seeking with accelerator algorithm. We consider the fastest version of search and suppress algorithm (the step steering direction is reversed if the width of the island increases by the pre-specified threshold for a single dwell time). The first number in each entry represents the average suppression time and the second number between parentheses represents the standard deviation for 100 simulations. The extremum seeking with accelerator algorithm provides the fastest suppression time, followed by the extremum-seeking algorithm and finally the search and suppress algorithm.

5. Conclusions

Previous work on modelling of the effectiveness of ECCD in suppressing NTM islands has been extended to include the effects of modulation. Both the effect of the ECCD power modulation duty-cycle and the island-beam phase mismatch have been incorporated into the dynamic model of the island width. It has been illustrated through an in-depth simulation study how the proposed control-oriented NTM response model can play an important role in testing the performance of minimum-seeking ECCD control algorithms and in enhancing their effectiveness through proper tuning before experimental implementation. In addition to the well-established search and suppress control method, extremum seeking, a non-model-based adaptive control scheme, has been proposed as an effective method to suppress NTM islands by ECCD in tokamak plasmas. Without any knowledge of the system dynamics, both alignment and modulation parameters can be optimized in real time by extremum seeking to improve the efficiency of NTM stabilization by ECCD. The effectiveness of the extremum-seeking method in aligning the ECCD with the NTM-driven magnetic island and stabilizing the mode has been compared with that of the search and suppress method. It has been shown that the extremum-seeking method has the potential to reduce NTM suppression times. Moreover, it has also been illustrated that the availability of an even imperfect dynamic model for the ECCD-controlled island width (modified Rutherford equation + ECCD beam effectiveness) can be exploited to further reduce the suppression time by providing an estimate of the to-be-corrected misalignment based on noise measurements of the island width and growth rate. In addition, it has been shown that, unlike the search and suppress method, the extremum-seeking method has the ability of simultaneously optimizing additional parameters beyond island-beam alignment which also affect the efficiency of the current drive in stabilizing NTMs, such as the ECCD power modulation duty-cycle and the phase mismatch between the beam 'on-period' and the island O-point. The potential advantages of the extremum-seeking method arising from the simulation study have yet to be confirmed experimentally. The

study carried out within this work, which assumes fixed values for the ECCD peak current density and deposition width, can be easily extended to the case where the total driven current is kept at the maximum value allowed by the ECCD system while the deposition width is optimized in real time by the extremum-seeking controller and the peak current density is changed accordingly.

Acknowledgments

We gratefully acknowledge Dr. David A. Humphreys and Dr. Anders Wellander from General Atomics, San Diego, USA, for helpful discussions. This material is based upon work supported by the National Science Foundation under CAREER award ECCS-0645086.

References

- [1] Buttery R.J. *et al* 2003 *Nucl. Fusion* **43** 69
- [2] Halpern F.D., Bateman G. and Kritz A.H. 2006 *Phys. Plasmas* **13** 062510
- [3] Hegna C.C. and Callen J.D. 1997 *Phys. Plasmas* **4** 2940
- [4] Zohm H. 1997 *Phys. Plasmas* **4** 3433
- [5] Zohm H. *et al* 1999 *Nucl. Fusion* **39** 577
- [6] Zohm H. *et al* 2001 *Nucl. Fusion* **41** 191
- [7] Gantenbein G. *et al* 2000 *Phys. Rev. Lett.* **85** 1242
- [8] Lahaye R.J. *et al* 2002 *Phys. Plasmas* **9** 2051
- [9] Prater R. *et al* 2003 *Nucl. Fusion* **43** 1128
- [10] Isayama A. *et al* 2000 *Plasma Phys. Control. Fusion* **42** L37
- [11] Maraschek M., Gantenbein G., Yu Q., Zohm H., Günter S., Leuterer F., Manini A., ECRH Group and ASDEX Upgrade Team 2007 *Phys. Rev. Lett.* **98** 025005
- [12] Woodby J., Schuster E., Bateman G. and Kritz A.H. 2008 *Phys. Plasmas* **15** 092504
- [13] Perkins F.W., Harvey R.W., Makowski M. and Rosenbluth M.N. 1997 Prospects for electron cyclotron current drive stabilization of neoclassical tearing modes in ITER *Proc. 17th IEEE/NPSS Symp. on Fusion Engineering (San Diego, California, 6–10 October 1997)* vol 2 pp 749–51 <http://ieeexplore.ieee.org/xpl/articleDetails.jsp?arnumber=687734>
- [14] Giruzzi G., Zabiégo M., Gianakon T.A., Garbet X., Cardinali A. and Bernabel S. 1999 *Nucl. Fusion* **39** 107
- [15] Yu Q., Zhang X.D. and Gunter S. 2004 *Phys. Plasmas* **11** 1960
- [16] La Haye R.J. *et al* 2005 *Nucl. Fusion* **45** L37
- [17] Humphreys D.A., Ferron J.R., La Haye R.J., Luce T.C., Petty C.C., Prater R. and Wellander A.S. 2006 *Phys. Plasmas* **13** 056113
- [18] Wehner W. and Schuster E. 2009 Stabilization of neoclassical tearing modes in tokamak fusion plasmas via extremum seeking *Proc. 18th IEEE Int. Conf. on Control Applications (Part of 2009 IEEE Multiconference on Systems and Control) (Saint Petersburg, Russia, 8–10 July 2009)* pp 853–60 <http://ieeexplore.ieee.org/xpls/abs.all.jsp?arnumber=5280943>
- [19] La Haye R.J. 2006 *Phys. Plasmas* **13** 055501
- [20] Wilson H.R. 2008 *Trans. Fusion Sci. Technol.* **53** 152 www.new.ans.org/pubs/journals/tst/a.1701
- [21] Sauter O. 2004 *Phys. Plasmas* **11** 4808
- [22] Volpe F.A.G., Austin M.E., La Haye R.J., Lohr J., Prater R., Strait E.J. and Wellander A.S. 2009 *Phys. Plasmas* **16** 102502
- [23] Ariyur K. and Krstic M. 2003 *Real-Time Optimization by Extremum Seeking Feedback* (New York: Wiley)
- [24] Krstic M. and Wang H.-H. 2000 *Automatica* **36** 595
- [25] Takata H., Hachino T., Tamura R. and Komatsu K. 2005 *IEICE Trans. Fundam.* **E88-A** 2535